Demonstrate A Two-qubit Gate with an Ultracold Atoms System

Ph.D research proposal by Yanay Florshaim

Advisor: Prof. Yoav Sagi

May 30, 2018

Department of Physics

Technion - Israel Institute of Technology

Abstract

This research proposal offer implementation of a new method of a two-qubit gate in ultracold fermionic system. This method is based on the experimental toolbox in ultracold atom apparatus and the fermionic statistic. We offer a $\sqrt{\text{SWAP}}$ gate protocol that can give to such system the ability to break the limit of quantum computation. As i describe in this proposal, the new platform based on ultracold ^{40}K fermionic atoms held in an optical microtrap. The quantum information can be stored in the internal states of these atoms or in vibrational states of the trap.The universal two-qubit $\sqrt{\text{SWAP}}$ gate can be implemented by a novel protocol that takes advantage of our ability to precisely control the tunneling energy and the interaction energy (by using Feshbach resonance) between two atoms at two adjacent traps. I present our new apparatus design and describe the open questions for my Ph.D. research.

Contents

1 Introduction

This section provides a short introduction and then introduces a motivation and the condition of quantum computation.

1.1 Ultracold atoms

Ultracold atomic gases provide quantum systems of exceptional purity and offer almost complete experimental control. Not only is it possible to prepare the atoms in a well-defined internal state, but also can the external motion be cooled until it reaches its ground state. In such systems, we can divide the cooling process to a two parts. First, an on-resonance laser is used to cool the atoms to approximately $10\,\mu$K in ^{40}K. Then, the cooling part includes evaporation in a magnetic trap and optical trap. One of the important tools in such systems is the ability to tune the interaction from strongly repulsive to attractive by an external magnetic field.

1.1.1 Feshbach resonance in cold atoms

One of the experimental tools in ultracold atom experiments is controlling the interaction between atoms using the Feshbach resonance mechanism. The mechanism can widely tune the interaction between two atoms and can be described as a scattering process that depends on a single parameter — the scattering length that is given by

$$a = -\lim_{k \ll 1/r_0} \frac{\tan(\delta_0)}{k}$$

where k is the scattered atom momenta, r_0 is the interaction range, and δ_0 is the phase shift between the incoming and the scattered wave-functions. For alkali atoms (such as ^{40}K), the scattering length is around the van der Waals atomic range $a \sim r_0 = 50 - 100a_0$, where a_0 is the Bohr radius. In this case, $1/k_F a \approx 0.03$, which is very small compared to weakly interacting gas. The scattering length can be tuned from negative to positive, making the atoms vary from attractive to repulsive, respectively.
The key to manipulating the scattering length stems from the coupling between different atomic states with different total magnetic moments. The relative offset moments between the different state can be tuned via an external magnetic field based on their different magnetic moments (Zeeman shift). Typically, the atoms enter the collision in the lowest energy channels, which are called open channels. The second method uses closed channels, which have higher energies.

The relative Zeeman shifts between these two channels can be used to tune the energy of the last bound state of the closed channel into resonance with the close channel bound state. As a result, the scattering length diverges at resonance and is given by the following:

$$a(B) = a_{bg}\left(1 - \frac{\Delta B}{B - B_0}\right) \tag{1}$$

where a_{bg} is the background scattering length away from resonance, ΔB is the resonance width, and B_0 is the resonance position. In ^{40}K, the parameters for Feshbach resonance between the states $|F = 9/2, m_f = -9/2\rangle$ and $|F = 9/2, m_f = -7/2\rangle$ are: $a_{bg} = 169.7 a_0$, $B_0 = 202.14\,(1)$ G, $\Delta B = 6.70\,(3)$ G. There is more resonance between other states, but with these states, there is a possibility of spin-exchange collisions.

1.1.2 Optical dipole trap

Another powerful experimental tool is the ability to trapped and manipulate atoms in an optical trap. In this section, I will describe the mechanism of optical trap in cold atoms system.

When an electric field $\vec{E}$ oscillating with frequency ω, such as the light field, acts on a neutral atom, it induces an electric dipole moment

$$p = \alpha E$$

where α is the complex polarizability. Because this electric dipole moment interacts with the light field, the atom has a potential energy of

$$U_{dip} = -\frac{1}{2}\langle pE \rangle \propto -\text{Re}\,(\alpha)\,|E|^2$$

Therefore, the potential energy is proportional to the intensity $I \propto |E|^2$ of the oscillating field. Considering the frequency dependence of and damping due to spontaneous emission, the full expression for the dipole potential is given by [13]:

$$U_{dip}(r) = \frac{3\pi c^2 \Gamma}{2\hbar \omega_{0,1}^3 \delta} I\,(r) \tag{2}$$

where $I\,(r)$ is the laser beam intensity, Γ is the natural line-width, and $\delta = \omega - \omega_{0,1}$ is the frequency detuning of the laser from the frequency of the optical transition $\omega_{0,1}$. The dipole trap can be attractive for red detuning ($\delta < 0$) or repulsive for blue detuning ($\delta > 0$). For the simple case of TEM$_{00}$ Gaussian mode, the depth of the potential is given by

$$U_{dip}(r, z) = -U_0 \left[1 - 2\,(r/\omega_0)^2 - (z/z_R)^2\right]$$

where ω_0 is the beam waist, z_r is the Rayleigh range, and U_0 is the trap depth.

1.2 Quantum computation and simulation

In quantum mechanics, the dimension of the Hilbert space grows exponentially with the system size. In order to present a quantum state with n particles in classical computation we need an order of C^n bytes, where C is a constant. Therefore, the possibility of calculating many-body quantum states becomes an impossible situation in classical computing.

To overcome this problem, Richard Feynman first proposed to use a quantum computational machine ("Quantum Computer")[11]. A quantum computer can simulate quantum dynamics and complex mathematical problems.

For two decades, researchers have been trying to implement quantum computation using different platforms. These platforms have made progress, but all these systems have been limited and need further

development.

Quantum computer system requirements as stated by D.DiVincenzo [9] should comply with five conditions:

- **Quantum state.** The quantum state is the storage of the quantum information in a quantum computer; therefore it needs to be defined well. In quantum computation two states are usually used, $|0\rangle$ and $|1\rangle$. These states define the qubit, and the qubit state is defined by

$$|\psi\rangle = \alpha |0\rangle + \beta |1\rangle$$

where α and β are complex numbers. When the qubit is measured, the probability of it being in state $|0\rangle$ is determined by $|\alpha|^2$ and the probability of it being in state $|1\rangle$ is determined by $|\beta|^2$, satisfying the following relation:

$$|\alpha|^2 + |\beta|^2 = 1$$

since the probabilities must total one.

- **Preparation of the Initial State.** The system should have the possibility to prepare the initial state of the qubit. The initial state is of little importance as we can enable operators ("quantum gates") to function upon the system, obtain every possible state, and use each state as an initial base for the system.

- **Quantum Gates.** It should be possible to operate the system with a set of operators. The system should include the possibility of performing on several universal unitary operations ("Quantum Gates"), and a gate can act on a one-qubit or a two-qubit system. There are several types of one-qubit gates such as a Hadamard gate, a phase gate, and a $\pi/8$ gate. The two-qubit gate is C-NOT. In place of a C-NOT, a $\sqrt{\text{SWAP}}$ gate can be used.
By using Hadamard, Phase, and $\sqrt{\text{SWAP}}$ gates, any unitary operation of n qubits can be obtained by taking a cumulative series of these gates.

- **Ability to Measure the Result.** The ability to measure the final state of the system is required for all computation systems. Therefore, the measurement technique should provide an ability to distinguish between the qubits and its state.

- **System Scalability.** System physical resources (e.g., space and money) do not scale as X^n, where X is some system constant and n is the number of qubits. This requirement enables the system to become technically effective.

Another problem that exists in the real world is decoherence due to undesirable interactions between the quantum computer and its environment. Therefore, the time scale of the system isolation T_I must be smaller than the preparation time of all the operation T_{gate}.

$$\frac{T_{gate}}{T_I} \ll 1$$

To date, attempts have been made to create different physical systems to meet these requirements, including optic [23], ion traps [7, 15], quantum dots [17], neutral atoms in optic trap [30], and superconductivity devices [2]. All of these systems suffer from inherent limitations that prevent them from constituting a perfect platform for quantum computation. For example, in an ion trap, charged ions can be heated by fluctuating patch potentials in trap electrodes [31].

We have developed a new platform of quantum computation that is based on ultracold fermionic atom in an optical microtrap. The basis for these platforms is that the system has a fermionic statistic. In addition, the system of cold atoms can control the interaction between atoms by using Feshbach resonance. Furthermore, the depth of the micro-trap, shape, and position in space can be controlled dynamically.

2 The new platform of quantum computation

This chapter describes how the five conditions for quantum computation are realized in the proposed computational scheme. The $\sqrt{\text{SWAP}}$ gate was developed by Dr. Jonathan Nemirovsky.

2.1 The qubit

The proposed quantum computer is based on two internal energy levels of a ^{40}K atom held in a microtrap. The states $|\downarrow\rangle = |0, 9/2, -9/2\rangle$ and $|\uparrow\rangle = |0, 9/2, -7/2\rangle$ with notation $|n, F, m_f\rangle$, where n is the vibrational state, F is the total atomic spin, and m_f is the projection in $\hat{z}$ direction (set by external magnetic field). Any two m_f states could be used, but the interaction between the atoms was controlled by means of a Feshbach resonance [6]. The Feshbach resonance between $m_f = -9/2$ and $m_f = -7/2$ was at $B = 202.14$ G, and this tunability is important for implementing the two-qubit gate (for more detail see section 2.3).

2.2 Preparation initial state

The requirement of preparation sequence is to generate a single atom in a microtrap with the ability to

know the initial state. The particular initial state is of little importance, as it can be transformed to any other state using several quantum gates. However, it is important that the initial state can be created with high fidelity. The system is described in more details in section (4.1).

2.3 Quantum Gate

To perform a quantum computer, a single-qubit gate and the two-qubit gate (**Hadamard** gate, the phase gate, $\boldsymbol{\pi/8}$ gate) and the two-qubit gate $\sqrt{\text{SWAP}}$ was used in the proposed system.

- Single qubit gate:
  Any unitary transformation on a single qubit can be decomposed into a rotation in the Bloch sphere around some axis $\hat{n}$ by an angle θ multiplied by a global phase ϕ

$$U = e^{i\phi} e^{-i\frac{\theta}{2}\cdot\hat{\sigma}_n}$$

  where $\hat{\sigma}_n$ is Pauli matrices. This unitary transformation can be realized in a ultracold atoms system by coupling some two-level system to an external Electromagnetic field [1, 18]. The experimental parameters that control the Bloch sphere rotation are the phase of the RF pulse and the detuning between its frequency and the two different energy states divided by $\hbar$.

- $\sqrt{\text{SWAP}}$ gate
  The $\sqrt{\text{SWAP}}$ is a two-qubit gate that swaps the states half way, namely,

$$U_{\sqrt{swap}} = \begin{bmatrix} 1 & 0 & 0 & 0 \\ 0 & \frac{1}{2}(1+i) & \frac{1}{2}(1-i) & 0 \\ 0 & \frac{1}{2}(1-i) & \frac{1}{2}(1+i) & 0 \\ 0 & 0 & 0 & 1 \end{bmatrix}$$

  with respect to the basis $|\downarrow\downarrow\rangle$, $|\downarrow\uparrow\rangle$, $|\uparrow\downarrow\rangle$, $|\uparrow\uparrow\rangle$. In Bell state representation, the $\sqrt{\text{SWAP}}$ only changes the anti-symmetric state to

$$\left(\hat{d_1}^\dagger \hat{u_2}^\dagger - \hat{u_1}^\dagger \hat{d_2}^\dagger\right)|\psi\rangle \rightarrow i\left(\hat{d_1}^\dagger \hat{u_2}^\dagger - \hat{u_1}^\dagger \hat{d_2}^\dagger\right)|\psi\rangle$$

  whereas no other states are developed.
  To implement the two-qubit $\sqrt{\text{SWAP}}$ gate, two unique advantages of ultracold atoms were utilized.

    - Ability to control the interaction between atoms around the Feshbach resonance [6].
    - Ability to shape the potential landscape using far off resonance light, controlling the atom tunnel-

ing between two traps [27].

advantages, together with fermionic statistics, are the basis for a new protocol for the $\sqrt{\text{SWAP}}$ gate. This protocol is original but similar in some aspects to the gate first described in Ref. [14]. Two optical microtraps with one atom at each site with a distance $d(t)$ between them. Using second quantization formalism and the Fermi-Hubbard model [16], the Hamiltonian is given by

$$H_{J,U} = J \cdot \left(\hat{u}_1^\dagger \hat{u}_2 + \hat{u}_2^\dagger \hat{u}_1 + \hat{d}_1^\dagger \hat{d}_2 + \hat{d}_2^\dagger \hat{d}_1 \right) + 2U \cdot \left(\hat{u}_1^\dagger \hat{u}_1 \hat{d}_1^\dagger \hat{d}_1 + \hat{u}_2^\dagger \hat{u}_2 \hat{d}_2^\dagger \hat{d}_2 \right)$$
$$\equiv J \cdot H_J + U \cdot H_u$$

Where J is the tunneling energy, U is on site interaction energy, $\hat{u}_i$ and $\hat{u}_i^\dagger$ are annihilation and creation operators of particle i in state $|\uparrow\rangle$, and $\hat{d}_i$ and $\hat{d}_i^\dagger$ are annihilation and creation operators of particle i in state $|\downarrow\rangle$. By tunning the system parameters $U = U_1$ with Feshbach resonance and $J = J_1$ with the distance between the qubits $d(t)$ and set the gate duration as T_1, the dynamics of the Hamiltonian are given by

$$\sqrt{\text{SWAP}} = \exp\left(-iT_1 H(U_1, J_1)/\hbar\right)$$

The conditions on U_1 and T_1 are:

$$U_1 = \pm \frac{2J\hbar \left(2n - \frac{1}{2}\right)}{\sqrt{m^2 - \left(2n - \frac{1}{2}\right)^2}} \qquad\qquad T_1 = \frac{\hbar\pi \sqrt{m^2 - \left(2n - \frac{1}{2}\right)^2}}{2J}$$

Where m is an odd integer and n is any integer. The last parameter, J_1, depends on the distance between the two-qubits, i.e., $d(t)$.

The $\sqrt{\text{SWAP}}$ gate can be realized in the following stages.

1. The tunneling was set to some value $J = J_1$ and the interaction was determined to be $U = 0$. Then, after $t_1 = \frac{\pi\hbar}{4J_1}$, the dynamic for the anti-symmetric state $|\psi_A\rangle$ state was obtained.

$$\left(\hat{d}_1^{\dagger} \hat{u}_2^{\dagger} - \hat{u}_1^{\dagger} \hat{d}_2^{\dagger} \right) |0\rangle \rightarrow -i \left(\hat{d}_1^{\dagger} \hat{u}_1^{\dagger} + \hat{u}_2^{\dagger} \hat{d}_2^{\dagger} \right) |0\rangle .$$

while the symmetric states $\hat{d}_1^{\dagger} \hat{u}_2^{\dagger} + \hat{u}_1^{\dagger} \hat{d}_2^{\dagger}$, $\hat{u}_1^{\dagger} \hat{u}_2^{\dagger}$, $\hat{d}_1^{\dagger} \hat{d}_2^{\dagger}$ are stationary.

2. In addition, the tunneling energy was set to zero, $J = 0$ and the interaction $U = U_1$ for a duration

6

Figure 1: Calculation of J vs. NA for difference distance. For this calculation the traps prameters are $\lambda = 1064$ nm, and each trap depth is $V_0/k_b = 310$ nK. This 3D numerical calculation is done in Cartesian coordinates with 102 divisions at each dimension.

of $t_2 = \frac{\pi \hbar}{4U_1}$. As a result, the symmetric states do not change when the $|\psi_A\rangle$ state is now

$$-i\left(\hat{d_1}^\dagger \hat{u_1}^\dagger + \hat{u_2}^\dagger \hat{d_2}^\dagger\right)|0\rangle \rightarrow -\left(\hat{d_1}^\dagger \hat{u_1}^\dagger + \hat{u_2}^\dagger \hat{d_2}^\dagger\right)|0\rangle$$

3. The last stage repeats the first stage by setting the tunneling energy as $J = J_1$ and turns off the interaction. The waiting time was $t_1 = \frac{\pi \hbar}{4J_1}$, and the symmetric state, again, did not change

$$-\left(\hat{d_1}^\dagger \hat{u_1}^\dagger + \hat{u_2}^\dagger \hat{d_2}^\dagger\right)|0\rangle \rightarrow i\left(\hat{d_1}^\dagger \hat{u_2}^\dagger - \hat{u_1}^\dagger \hat{d_2}^\dagger\right)|0\rangle$$

which this is the $\sqrt{\text{SWAP}}$ gate. The gate duration $T = 2t_1 + t_2$, is proportional to U^{-1} and J^{-1} and therefore, the demand of shortening gate duration creates a requirement about U and J. The parameter U is determinate by an external magnetic field, while the J is determined by the overlap between the two atoms wave function and can be calculated by a difference between the symmetric and the anti-symmetric energy.

$$J = \frac{E_{\text{sym}} - E_{\text{anti}}}{2}$$

We make a numerical calculation of a 3D Gaussian double well and calculate J vs. NA (that set the potential parameters) and the distance between the microtrap figure 123. The tunneling is .....

2.4 Detection

After the atoms are encoded, their final state must be detected. A single ^{40}K atom cannot be detected for atoms in optical trap with fluorescence imaging on the cycling transition$|-9/2, -9/2\rangle_{^2S_{1/2}} \rightarrow |11/2, -11/2\rangle_{^2P_{3/2}}$ due to the $3D_{3/2}$ transition (1169 nm from the $^2P_{3/2}$) [5]. In the recent years, some groups developed new techniques of single potassium detection.In the recent years, some groups developed new techniques of single potassium detection. In section section 4.3 , is described three methods to detect a single ^{40}K.

2.5   Scalability

The scalability in our scheme is fairly straightforward. The cooling sequence is the same and does not require any more resources, and more micro-trap can be loaded from the same ensemble. The position of each qubit depends on the angle beam that translates by the objective to a position in the focal plane. The distance between the trap is given by

$$\theta = f \cdot d$$

Where d is the distance between two microtraps and f is the objective focal length. One way to control dynamically the relative angle θ is to use Acousto-Optic-Deflector (AOD). By placing two AOD in an orthogonal direction, the position of the microtraps in the focal plane plane can be moved in two dimensions [19].
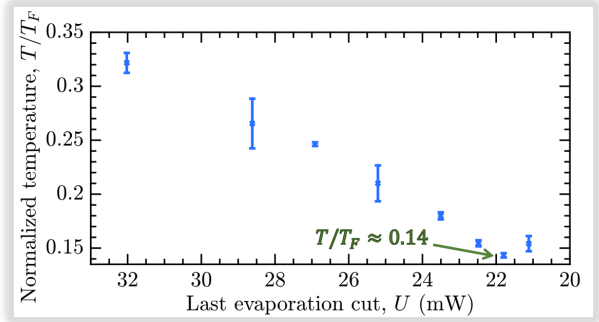
3   Preliminary Results

Over the past three years, I have been an important partner in the development of the first cold-atom system of Prof. Yoav Sagi group. In this system (which was built for other requirements), the method for the new apparatus was checked. All the preliminary results were performed on the first system that composed of three cells under ultrahigh vacuum (2). In the first cell (source), ^{40}K atoms are released from homemade dispensers and immediately captured by a 2D Magneto optical trap (MOT). On the third axis, there is a mirror with a hole (nozzle) inside the chamber. The atoms are cooled in two axes and pushed to the second cell by another laser. In the second chamber (cooling), the atoms are captured by a 3D MOT. At this point, the atoms cloud temperature is around 220 μK. By using a gray molasses cooling on the D_1 transition, the atomic cloud temperature is reduced to approximately 15 μK. Next, the atoms are optically pumped into the states $|9/2, 9/2\rangle$ and $|9/2, 7/2\rangle$ and loaded into a QUIC magnetic trap. In this configuration, a magnetic trap a zero magnetic field is obtained (this is important for RF evaporation). Following the evaporation, the temperature is $T/T_f \approx 4.5$. Next, the atoms are loaded into a far-off-resonance optical trap that focuses to 39.5 μm with a power of 6W. The optical trap is moved adiabatically by the air-bearing stage to the science chamber, which is distance of 320 mm. During the movement, the trap waist drops to 19.5 μm and increases the trap depth. Therefore,the laster beam power is lowered and evaporates in the movement. In the science chamber, a second beam crosses the first beam at an angle of 45° with $\omega_0 = 200 \,\mu$m with power of 2.8 W. Finally, the optical evaporation continues to 10 mW in the main beam and 1.5 W in the cross beam. The conditions at the end of the preparation process are ~150,000 atom per spin state at $T/T_F \approx 0.2$.

3.1   Creating and loading a micro trap

One of the most parts of our system is the ability to create a single atom in ground state hold in optical micro-trap. In the new system, an objective with high NA is needed (>0.6). In order to learn the ability to load a single atom in a trap, we constructed an objective with NA=0.3 that designed for our existing
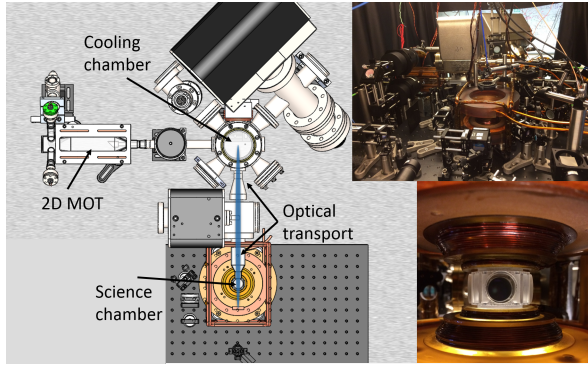
Figure 2: (a) The preliminary results experimental system. A top view of the three chamber design. The cooling process starts in the 2D MOT chamber, where a stream of cold ^{40}K atoms is generated towards the cooling chamber. In the cooling chamber, the atoms are cooled using a 3D MOT and D1 cooling. Then, the atoms are loaded into a QUIC magnetic trap, where MW evaporation is performed. The evaporation stops at $T/T_F \approx 4.5$ and then the atoms are loaded to an optical trap. The atoms are transferred to the science chamber by moving a lens on an air-bearing stage. The science chamber allows for excellent NA of 0.75 in one axis. (b) The final conditions of the atoms vs. optical trap cutoff evaporation.

Surface number	Catalog number	Radius [mm]	Distance to the next surface [mm]	Material
1	LC1582	∞	3.5	BK7
2	-	38.6	10.92	air
3	LB1901	76.6	4.1	BK7
4		-76.6	10	air
5	LA1608	38.6	4.1	BK7
6		∞	2	air
7	LE1234	32.1	3.6	BK7
8		82.2	21	air
9	Vacuum window	∞	3.15	Silica
10		∞	-	Vacuum

Table 1: Technical detail of the lenses. All the lenses are commercial from the Thorlabs catalog.

apparatus.

3.1.1   Homemade objective with NA=0.3

The proposed simulation was used for ray trace to design a homemade objective from four commercial lenses shown in Table (1). Figure 3a, the proposed simulation found the maximum NA=0.3 with $\lambda = 1064$ nm. A holder from Ultem with a spacer from aluminum was designed and created. The aluminum spacer took out after the lens position was fixed by glue. The objective was characterized by two independent measurements. First, the waist ω_0 was measured to describe the numerical aperture of the objective. A knife edge measured with a resolution of ~ 50 nm (with Michelson interferometer) and get $\omega_0 = 2.35\,\mu$m was created (4). Second, the resolution was measured by looking at the resolution target measuring the point-spread-function (PSF) of 1 μm pinhole. A 1951 USAF resolution target was used and magnified the imaging by 28 on a CCD camera. A resolution of 4.4 μm was used, and a higher resolution was observed when a laser 770 nm was used (the original design was for 1064 nm). Using this system, the PSF can be measured from a pinhole of $1.25 \pm 0.25\mu$m. A NA $= 0.258 \pm 0.03$ for PSF fitting and NA NA $= 0.289 \pm 0.0083$ were used for modulation transfer function calculation which is the mathematical Fourier transform of the PSF figure 4b.

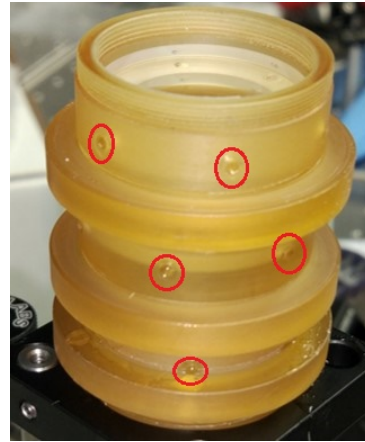### 3.1.2   Loading a single atom to microtrap

One of the demands of our system is the ability to create a single atom in the ground state. In degenerate Fermi gas, the occupation probability for a state with energy E is described by Fermi-Dirac statistics

$$P\left(E\right) = \frac{1}{\exp\left(\frac{E-\mu}{k_B T}\right) + 1}$$

where μ is the chemical potential, k_b is a Boltzmann constant, and T is the temperature. To calculate this
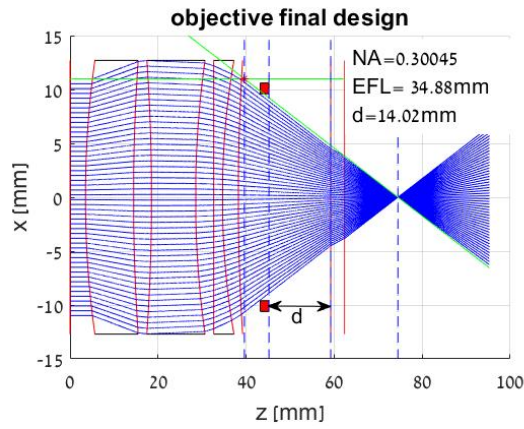
Figure 3: (a) Computer simulation of the Objective's performance (MATLAB). The simulation predicted a $NA = 0.3$ and an effective focal length of 34.88 mm, which yields a diffraction limit of $\omega_0 = 1.12$ μm for $\lambda = 1064$ mm. This calculation considers the vacuum window thickness and the distance of the atoms from the window. As a result, the distance between the final holder (red box) to the window is 14.02 mm. (b) Picture of the objective after assembly. The small holes are designed to attach holding lenses and thus allow the removal of the holders of the lenses (red circles). As a result, we take advantage of the whole size of the lenses and improve the NA.
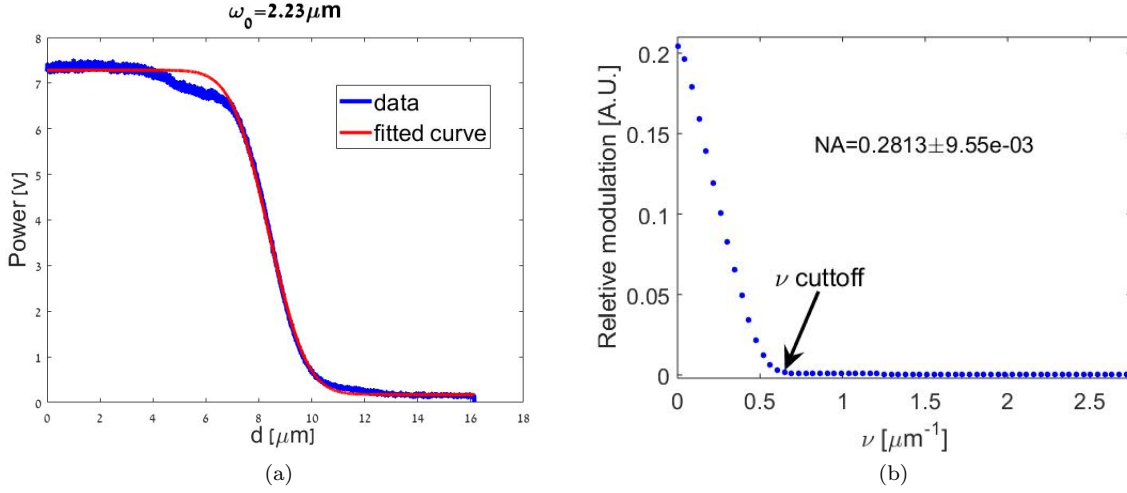
11

Figure 4: (a) Calculation of the beam waist with the knife edge technique. We calibrate the knife distance by using a Michelson interferometer. (b) MTF vs. frequency. The cutoff frequency is where the MTF is on the order of the noise.

probability, $\mu \approx E_F = k_B T_F^{reservoare}$ was used to change the optical trap parameters ($T_F^{microtrap}$ and the ground state energy $E_0 = \hbar\overline{\omega}$) such that

$$P(E_0) > 0.999$$

We can assume the number of atoms that load to the microtrap. The number state for Fermionic atoms is given by

$$N = \int_0^{U_{max}} n(\epsilon) g(\epsilon) d\epsilon$$

where U_{max} is the trap depth, $n(\epsilon) = \left(\exp\left(\frac{\epsilon-\mu}{k_B T}\right) + 1\right)^{-1}$ is the Fermi Dirac distribution, $g(\epsilon)$ is the atoms density. In 3D with a harmonic oscillator approximation, the atoms density is given by

$$g(\epsilon) = \frac{\epsilon^2}{2 h^3 \nu_x \nu_y \nu_z}$$

where ν_i is the optical trap frequency in axis $\hat{i}$. The temperature T and the chemical potential μ was measured by taking an absorption imaging before the microtrap is turn on and the potential parameters, U_{max} and ν_i was analytically calculated from the potential shape equation (2). In our trap parameters, The calculated number of state is 12 states for power of 15 μW and $\omega_0 = 2.35$ and 2000 states for power of 100 μW. This

12

The system was prepped as describe above with 300,000 atoms in $T/T_F \approx 0.4$. Then, the microtrap turn on and approximately 2000 atoms were loaded. Then, the microtrap laser power was lowered until$\sim$ 200 atoms were obtained. Afterwards, gradient coils were added to lower the total potential without changing the trap frequencies. To load the colder atoms, the trap and the microtrap need to be at the same position. First, a power of approximately 200 mW was used, and an iris inserted before the objective. As a result, high trap depth and more volume were obtained in the microtrap. As shown in figure 5, the microtrap position is found by taking absorption imaging of the atoms in the microtrap. In these conditions, approximately 40,000 atoms were loaded. Then, the iris was opened to lower the trap depth and scan the the trap position with a three axes translation stage. Because the absorption signal of a single atom is low, this method can not be used for measuring less than 4000 atoms. Therefore, the measurements were taken by 3D MOT as described in the following section. In the microtrap, the atoms lifetime is 26 sec,figure 6.
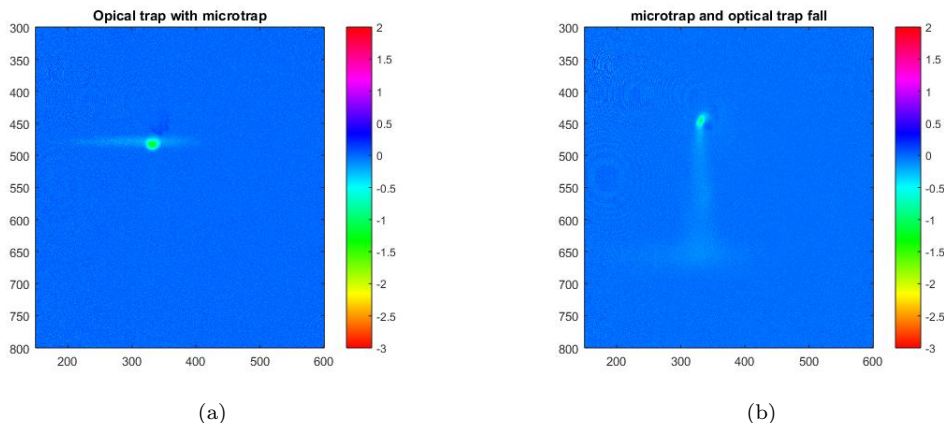

Figure 5: The microtrap positions were set to take the absorption imaging of the atoms cloud. In Figure (a), the traps are released at the same time, while in Figure (b), a delay of 10 msec is between them. The figures show that the atoms that are trapped in the microtrap stay at the same position while the rest are falling due to the gravitation force.

This research builds a single atom detection using 3D MOT, and the MOT parameters are different from the 3D MOT in the first cooling stage. For example, to localize the atoms in a small area, the magnetic field gradient is higher and the laser frequency detuning is smaller. The photons were collected by lens ($f = 75$ mm) with an NA of 0.17 to the sCMOS camera (Andor Zyla 5.5).The signal per atom in our system was calculated as 2700 $\frac{\text{count}}{\text{atom sec}}$. Unfortunately, the background scattering photons from the chamber windows is large ($\sim 5\%$ per surface), and the ability to detected atoms is limited to approximately 5 atoms. To overcome this limit, an ultra-narrow band-pass filter that blocks the D_2 photons and the D_1 photons were
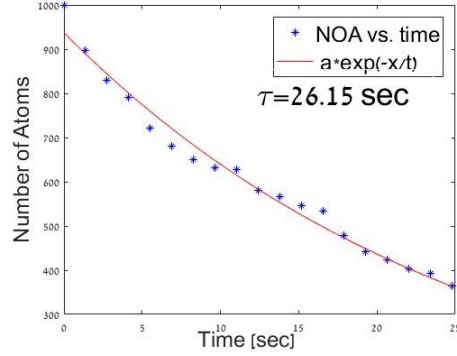
Figure 6: Measurement of the atoms lifetime in the microtrap

transited, was insert to the imaging system. First, a laser with a wavelength of the D_1 cooling was added, lowering the signal for the same number of atoms with the same lifetime (7). However, when a repump frequency was added to the MOT beam, almost the same signal as the D_2 3D MOT with a long life time. These new setups increased the SNR (for exposure time higher of 0.5 sec), and a single atom could be detected (7).
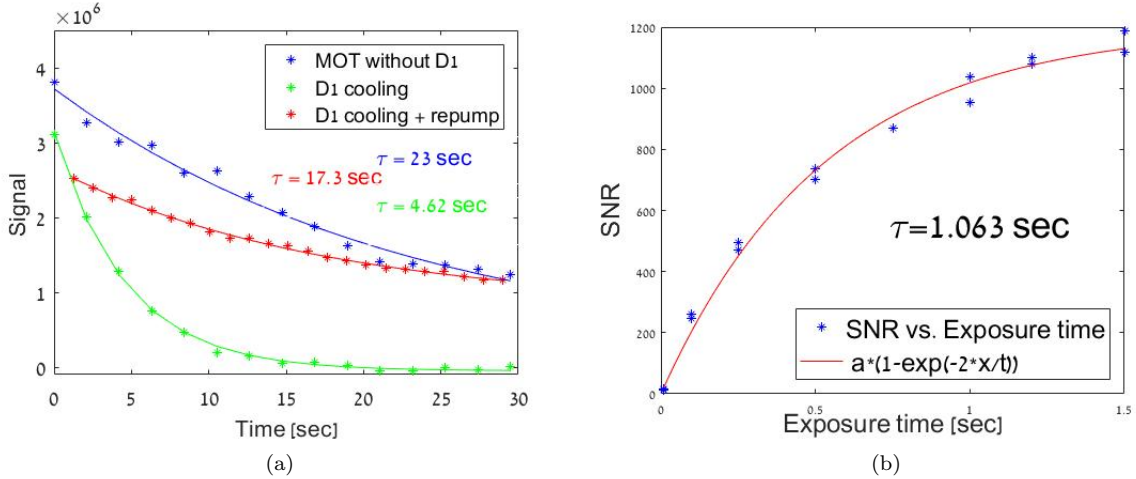

Figure 7: (a) Lifetime in 3D MOT. The 3D MOT on the D_2 is give a lifetime of 23 sec. The D_1 cooling is lower the lifetime while the D_1 repump can give the same signal and increase the lifetime to the regular MOT lifetime. The data was taken with the exposure time of 0.2 sec (b) SNR of the D_1 vs. exposure time.

In conclusion, We loaded several atoms to a microtrap with NA=0.3. Due to a high scattering background,

14

the detection was limited to approximately five atoms. The majority background comes from the science chamber window which design to other measurement techniques. To overcome this issue, a D_1 laser beam was inserted in the 3D MOT detection and raised the SNR with the same lifetime.

3.2 Sensitive RF Spectroscopy [28]

The 3D MOT adds the system a new detection ability of a small number of atoms. As a result, this research creates a measurement that requires a small number of atoms detection ability. One of these measurements is RF spectroscopy - a measurement of the number of atoms out-coupled by the RF pulse versus its frequency. From this measurement, many physical observables can be obtained. One of them is the contact C that measured the energy change due to the interaction energy between two fermions. At high frequency, contact interactions in 3D indicate a power-law of $\Gamma(\nu)$ [25].

$$\Gamma(\nu) \to \frac{C}{2^{3/2}\pi^2}\nu^{-3/2}$$

where ν is the rf frequency in unit of E_F/h and C is in unit of Nk_F, where N is the total number of atoms and k_F is the Fermi k-vector. In preliminary work, the signal was limited to $\nu < 12\ E_F$, and the signal of the contact is only above $5\ E_F$ [29]. Using the proposed RF spectroscopy scheme measures up to 150 - 200 E_F, opening a new tool to calibrate the interaction parameters and directly measuring the contact tail power law.

The atoms were prepared, as described previously, in a balance mixture of $|1\rangle = |F = 9/2, m_f = -9/2\rangle$ and $|2\rangle = |F = 9/2, m_f = -7/2\rangle$, which have Feshbach resonance at B = 202.2 G. The magnetic field decreased to B1 = 203.4 G at 30 ms and then after more 8 ms at B1 a 400 μs RF square pulse transfer a small fraction of atoms from state $|2\rangle \to |3\rangle = |F = 9/2, m_f = -5/2\rangle$ ($\sim$ 47 MHz depend on $B1$). a 3D MOT cannot be used simply to probe the $|3\rangle$ state without all the other states. Therefore, the atoms in $|3\rangle$ was transferred to $|4\rangle = |F = 7/2, m_f = -3/2\rangle$ with MW ramp. Due to their difference in the magnetic moment sign, the opening of magnetic gradient coils creates anti-trap potential for $|1\rangle$, $|2\rangle$, $|3\rangle$ states while $|4\rangle$ is trapped. Then, we wait a time that ensures that we stay just with $|4\rangle$ and open the 3D MOT. The signal of the atom was detection with a sCMOS Zyla 5.5 Andor camera.
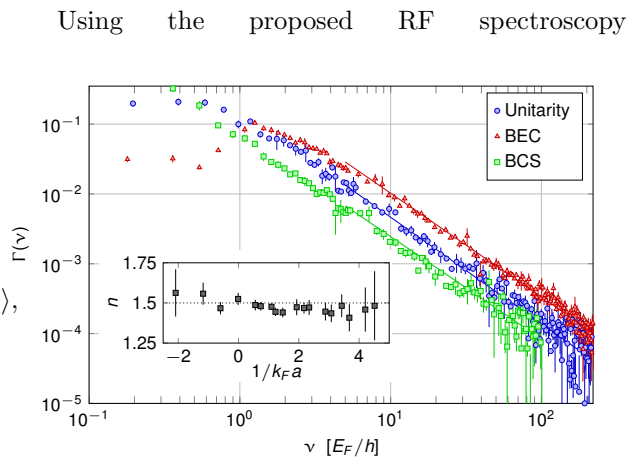

Figure 8: RF lineshapes for three different interaction strengths $1/k_Fa = 0$ (unitarity), $1/k_Fa = 0.49$ (BEC), and $1/k_Fa = -0.52$ (BCS) . Linear scaling shows that the data follows a power-law at high frequencies. The inset shows the power-law exponent extracted by fitting the tail of each dataset with c_1/ν^n.

16

Several line shapes were measured with different interaction strengths, and they were fit with a power law function $\Gamma(\nu) \propto \nu^{-n}$ (8). The results are compatible with the theoretical function with $n = 1.5$.

For an attractive force, we created a Feshbach molecule and measured their banning energy that given by

$$E_b = \frac{\hbar}{m(a - \bar{a})^2} \tag{3}$$

where $\bar{a}$ is the finite range correction of the van der Waals potential and a is the scattering length Eq.1. A general form of the transition line-shape of a weakly bound molecule is given by

$$\Gamma(\nu) = \Theta(\nu - E_b/h) \frac{C}{2^{3/2}\pi^2} \frac{\sqrt{\nu - E_b/h}}{(\nu - \nu_\omega)^2} \tag{4}$$

where Θ is the Heaviside step function. The data was fitted, showing a deviation from the previous ^{40}K parameters line that systematically increases from the data away from the resonance, which was unmeasured yet due to the low signal figure 7. The obtained data was fitted to calibrate the Feshbach resonance parameters $B_0 = 202.15\,(1)$ G and $\Delta = 6.70\,(3)$ G using the known values and $a_{bg} = 169.7\,a_0$ [10].

In conclusion, a new sensitive RF spectroscopy scheme in cold atoms was developed to open a new experimental research that have has a low signal of only several atoms. This method was applied to confirm the universal behavior of a contact-like potential. In addition, we calibrate the Feshbach resonance parameters B_0 and Δ were calibrated from the binding energy of the Feshbach molecule.

.

4 Research Plan

4.1 Dedicated New Experimental Apparatus

From the experience accumulated in our group over the last three years, the requirements of the new system can be accurately defined.

- **Short preparation time.**
  In quantum computation, the final state of mixed state with one measurement cannot be measured. For example, if the state is

  $$|\psi\rangle = \alpha\,|0\rangle + \beta\,|1\rangle,$$

  a single measurement gives a probability of $|\alpha|^2$ for $|0\rangle$ and with probability $|\beta|^2$ for $|1\rangle$. As described in Ref. [15], about 350 experiments were needed for each experimental value, e.g., a distance between the traps, the interaction, and the gate time. In the ultracold atoms system, each cooling stage takes a certain time; for example:
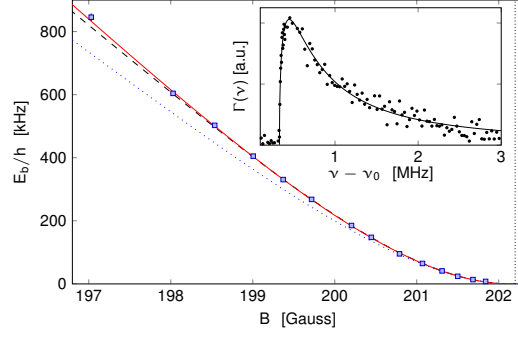
17

Figure 9: The binding energy of the Feshbach molecule at different magnetic fields close to the Feshbach resonance (202.2G). The binding energy (squares) were extracted by fitting the RF lineshape with the molecular spectral function given by Eq.4 (inset). The theory of equation 3 with the Feshbach resonance parameters given in Ref. [12]($B_0 = 202.20\,(2)$G, $\Delta = 7.04\,(10)$G, and $a_{bg} = 174a_0$) is a systematic divided from the experimental data (dotted blue line). The data was fitted to equation (3) with B_0 and Δ fit parameters (dashed black line). In addition, the data was fitted with a two coupled channels calculation (solid red line) based on the model of Ref. [26].

- 3D MOT loading - 20–50 sec
- D1 cooling - 10 msec
- Magnetic evaporation - 20–30 sec
- Optical evaporation - 3-5 sec

The preliminary result apparatus is shown in Section 3, the preparation time is approximately 70 sec. The total sequence duration for this system for 20 parameter points is

$$350 \cdot 20 \cdot 70 \approx 6\,\text{days}$$

Duration for such a long period cannot be ensured due to fluctuations in the magnetic field, laboratory temperature, lasers stability, and other properties of the lab. To ensure the measurement time is feasible, approximately 8 sec per measurement is needed.

- **A good separation between the atoms source chamber and the science chamber.**
  The atoms are released continually from a dispenser at a temperature of 300K and travel throughout all the vacuum chamber. To detect a single atom, there cannot be traveling atoms in the microtraps

18

area. These atoms shorter the lifetime in the optical trap, and we can not reduce their temperature low enough. In the first group apparatus, a three-chamber configuration was used. In the cooling chamber, all cooling processes performed include magnetic evaporation, and this system is not needed. Therefore, only one chamber is needed for releasing, while another chamber is needed to cooling and manipulate them.

- **High NA in one axis.**
  There are a number of reasons for the requirement to create a high NA at least on one axis. First, to load a single atom to a microtraps, an optical trap with ω_0 smaller than $1.8\,\mu$m is needed. Second, for the detection, a small number of photons are scattered by a single atom, and many as possible need to collect. Previous work obtains an apparatus with NA=0.86 with an objective with NA=0.6 and a hemisphere lens on the optical viewport [24]. The working distance in those works was $\sim 150\,\mu$m from the windows and; therefore, the entire beam must be within the total reflected angle to this surface. A new work with cesium used an objective with NA=0.92, but it was placed within the vacuum chamber [32]. Both techniques have a high NA but they insert a main constraint to the system, which is an undesired property. Section 4.2 describes a new method to use an objective with NA=0.65 which meets our requirements.

- **Avoid reflection photons scattering**.
  The first group apparatus uses a science chamber with a small optical window (but with high NA from 3 axes) and 5% reflection per surface. We suspect that overheating during baking caused the anti-reflection coating (AR) to be damaged. As a result, the scattering photons from the windows surface created a large background in the detection area. To avoid the large background, one axis with high NA will use, and all the other windows will take far from the position of the atoms. In addition, the vacuum system was baked up to $250°$ C to avoid any damage to the AR coating.

- **Ability to perform high magnetic field.**
  One of the main constraints in our system is the ability to control with high stability the interaction between two spin states. This is done by applying a magnetic field in the position of the atoms. As shown in section 1.1.1, the magnetic field needed for the proposed system is approximately 202.2+-7 Gauss (non-interaction is at 209G). Therefore, two coils with Helmholtz configuration were needed, and the chamber geometry determined the coil parameters (radius, distance from the atoms, and number of threads). We already perform a high stability current control (40 ppm) in our group.

By considering all these requirements, a new system containing two chambers was designed. One as a source and the second for a cooling and experimental place (10). Our apparatus is one long glass chamber ("2D chamber") that is connected to a hexagon chamber ("experimental chamber"). The entire system bakes to create an ultra-high vacuum ($\sim 10^{-11}$ torr). In addition, the science chamber is coated by a non-evaporable

getter (NEG) coating that can improve the vacuum. In the 2D chamber, ^{40}K atoms are released from homemade dispenser with a temperature of 300 K. Then, the atoms are trapped by a 2D MOT that creates a string of cold atoms. A laser beam in the third axis pushes the atoms through a nuzzle to the science chamber. The atoms are then collected and cooled in the experimental chamber by a 3D MOT. The 3D MOT consists of three counter-propagating circularly polarized beams with a retro-reflection configuration containing both cooling and repumping frequencies. The laser light at a wavelength of 767.7 nm for the cooling and repump is generated from two DBR lasers with tapered amplifiers. Both lasers are offset-locked relative to a common master laser which is stabilized using saturated absorption spectroscopy in a vapor cell containing ^{39}K. The temperature in 3D MOT is limited due to the Doppler limit

$$T_D = \frac{\hbar \Gamma}{2 k_B}$$

Where k_B is the Boltzmann's constant, $\hbar$ is the reduced Plank's constant, and Γ is the natural line-width [20]. In ^{40}K, the Doppler limit is $T_D = 145\,\mu$K. Then, gray molasses cooling are used on the D_1 transition to lower the atom temperature to approximately 15 μK. For the D_1 cooling, another DBR laser with a tapered amplifier is used. The laser is locked on the D_1 transition of the ^{39}K using saturated absorption spectroscopy (separated system from the D_2 transition locking system). The frequency is shifted ($\sim$705 MHz) to the cooling D1 transition in ^{40}K by using two Acousto-Optic-Modulatos (AOM). For the repump beam, we used the cooling beam and added a sideband by using a home-made, high-frequency electro-optic-modulator (EOM). The cooling and repump are phase locked, and this is necessary for D_1 cooling. Next,the atoms are loaded into an optical trap that is created by two lasers of 50 W at 1064 nm wavelength. This laser needs to be orthogonal with linear polarization. The laser focuses to $\omega_0 = 250\,\mu$m and interacts at an angle 14° at the center of the 3D MOT, creating a optical trap with $\sim 100\,\mu$K depth. Next, to evaporate the atoms, the optical depth is lowered up to $T/T_F \approx 0.5$. Then, we open the optical microtrap beam and load atoms to it (is presented in section 4.2). Finally, the microtrap power is reduced, and a gradient is opened to individually transport the atoms until one atom remains.

4.2   Microtrap

As shown in section 3.1.1, the first system already created a microtrap by using a home object with NA=0.3. In the initial numerical calculations of the $\sqrt{\text{SWAP}}$ gate, the NA must be large ($>$0.8) to obtain a short time scale for the gate. This demand is a result of the aspect ratio between the radial and the axial frequencies in a Gaussian beam. To apply this demand, an objective must be designed with a hemisphere lens on the vacuum chamber or designed to be in the vacuum chamber. To avoid building a system that is harmonized only to that without versatility, a new scheme is offered to overcome this problem when NA is 0.65. Optical trap frequencies are depended on the waist ω_0 in the radial axis and the Raleigh range z_R in
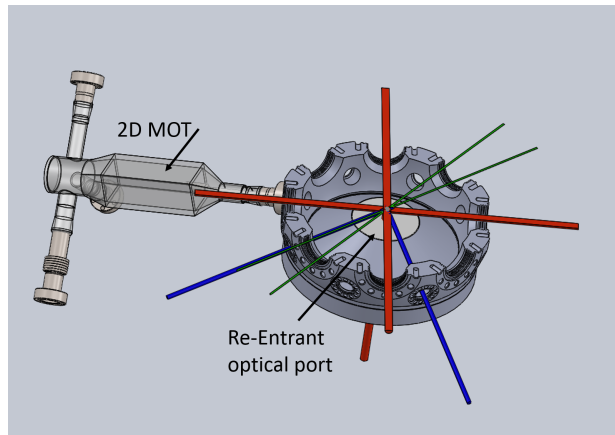
Figure 10: A 3D model of the new apparatus. The atoms are released and captured in a 2D MOT. In the experimental chamber, we apply a 3D MOT and D_1 cooling from three retro-reflection beams (red line). In addition, an optical trap is induced from two far resonance lasers with 6° between them (green line). The detection beams have an angle of 68° from z axis (blue line). This angle is important to RSC detection (see section 4.3). In the new apparatus, a working distance of approximately 12.5 nm was detected between the atom position and the last view port surface.

the longitudinal axis.

$$\nu_r \propto \frac{1}{\omega_0}, \qquad \nu_z \propto \frac{1}{z_R}$$

For given NA, the aspect ratio is given by $NA = \omega_0/z_R = \sqrt{2}\nu_z/\nu_r$, and as shown in figure 11, the aspect ratio can be less then 1.6 with NA>0.85. To overcome this experimentally difficulty, a standing wave in the longitudinal axis was added. The standing wave can be matched to the microtrap radial frequency, giving an aspect ratio$\sim$ 1.32 (which equivalent to NA=1.1). The standing wave is created from two laser beams 90 degrees from the microtrap longitudinal axis and separated by $\sim 8°$, creating 2D "pancakes" with a distance of $\sim 7.64\,\mu$m between them. As shown in figure 11, the standing wave potential cuts the z axis and creates a large effective NA.
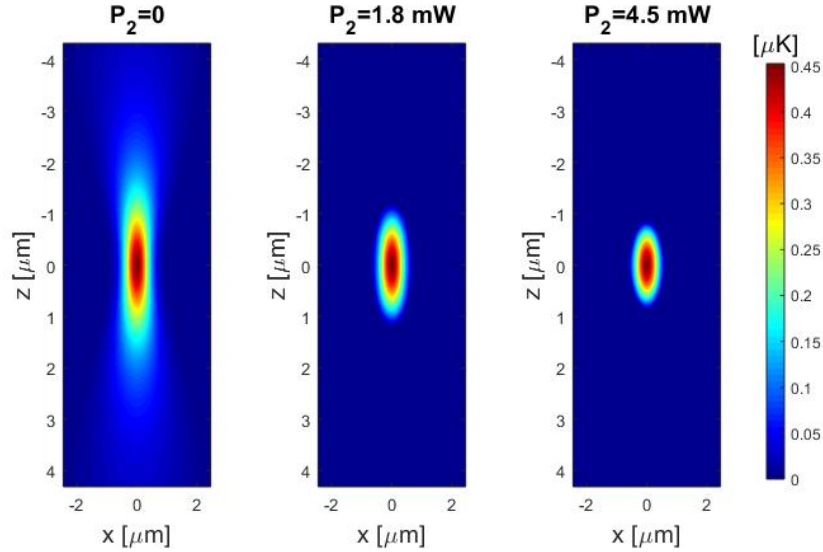

Figure 11: Microtrap potential vs. the second beam power. In the left figure, the potential depth was recorded without a second (standing wave) beam of a signal Gaussian beam with NA=0.65 and power of $2\,\mu$W. The standing wave beams were opened and quickly increased the aspect ratio between the Rayleigh range and ω_0 up to effective NA =1.1.

4.3   Single Atom Detection

The major open question is how to detect a single atom with spatial and the spin states resolved. In the last three years, there is a new technique of detecting single ^{40}K atoms. Each one of them has advantages and disadvantages as explained in the following section.

22

- Fluorescence detection.

  Fluorescence imaging cannot work for ^{40}K in optical lattice but may work for separated micro traps. Performing fluorescence imaging for ^6Li shows that fluorescence imaging of a single atom can work, but the spatial width of the signal is $\sim 5\ \mu$m [3]. For fluorescence imaging, the atomic sample can be illuminated from the size with two counter propagating laser beams. Then, the fluorescence photons can be captured with a high-resolution object in the orthogonal axis (the same objective that creates the microtrap). By inducing a magnetic field, the spin states are resolved. For example, for 204 G, the differences between $|-9/2, -9/2\rangle_{^2S_{1/2}} \to |11/2, -11/2\rangle_{^2P_{3/2}}$ and $|-9/2, -7/2\rangle_{^2S_{1/2}} \to |11/2, -9/2\rangle_{^2P_{3/2}}$ are $4\,\Gamma$ (25 MHz). The photon per atom is $\sim 60\ \text{photon}/\mu$s. To detect such low photon numbers with a single photon resolution, a camera camera with a high quantum efficiency needs to detect as many photons as possible. Furthermore, it is necessary that one photon creates a signal above the noise level. Consequently, an electron multiplying charged-coupled device (EMCCD) was used. .

- Ranam SideBand Detection.

  Raman sideband cooling was first proposed by Wineland in 1995, and it performed by using lasers and a magnetic field [22]. By adding a magnetic field, the relative energy between the vibrational state of two Zeeman sub-level are split such that the states $|F, m_f\rangle_n$ and $|F-1, m_f+1\rangle_{n-1}$ are degenerate (F represents the total spin number, m_f represents the Zeeman index, and n represents the vibrational state index). Then, by using a Raman transition, the atom can be pumped from $|F, m_f\rangle_n \longrightarrow |F-1, m_f+1\rangle_{n-1}$. The cooling cycle is completed by optically pumping the atom back to the initial state. To ensure that the atom pumps back to the initial state without changing its vibrational index, the Lamb-Dicke regime must be used. [8]. Only recently was it performed also with ^{40}K [5].

  By cooling with Raman sideband technique, the number of atoms at each site can be detected due to their fluorescence without heating. The fluorescence rate for single atom is $\sim 60-80$ photom/sec and can be measured with the EMCCD camera. The disadvantage of this technique is its incapability to distinguish between the atoms spin states and the complexity of its experimental system (lasers in D_1 and D_2 transitions that include four different frequencies).

- 3D-MOT Detection.

  Another way to detect a single atom with high fidelity is to use 3D MOT. Although this is the initial phase of cooling and heats the atoms to a temperature of T_D, it is an easy way to produce many of photons per atom. The key advantage over other detection schemes is that the observation time and therefore the number of collected photons can be made almost arbitrarily large. As show in section 3, the signal per atom with low NA (0.17) is approximately 2700 count/sec. Ultimately, it is only limited by the lifetime of the MOT, which is mainly determined by collisions with the background atoms. The disadvantage of this technique is that we can't get a spatially resolved detection. On the other hand, it does not require more lasers frequencies (we have these in the 3D MOT and D_1 cooling) and a high

quality camera.

4.4 Single atom interferometer

The computation scheme is based on the ability to move the microtrap and moreover without changing the atomic state included the phase between two qubits. In 1984, Berry finds that a cyclic evolution of a wave function adds a phase shift, and this phase shift is a sum of a dynamical phase and a geometric phase [4]. The difference in phase depends on the trajectory, and therefore each qubit gets a different phase depending on the path. One goal of this research is to find such trajectory to eliminate this phase difference. In our system, the final phase can be measured by creating a single atom interferometer. For the experiment, a single atom will be placed in a single trap in a $|\psi(0)\rangle = |\downarrow\rangle_{x1}$ state at x_1 and, then, a second microtrap at distance d opens. Over time $t_1 = \frac{\hbar J}{2}$, the wave packets will be localized at both microtraps.

$$|\psi(t_1)\rangle = \alpha_1 |\downarrow\rangle_{x_1} + \alpha_2 |\downarrow\rangle_{x_2}$$

Then, the microtrap at position x_2 is moved to x_1 with a wanted trajectory. This movement adds a relative phase between the two microtraps wave function

$$|\psi(t_f)\rangle = \alpha_1 |\downarrow\rangle_{x_1} + \alpha_2 e^{-i\theta} |\downarrow\rangle_{x_1}$$

The probability to measured the atoms is given by

$$p = \left|\alpha_1 + \alpha_2 e^{-i\theta}\right|^2$$
$$= \alpha_1^2 + \alpha_2^2 + 2\alpha_1\alpha_2 \cos(\theta)$$

By taking only the trajectory without a phase, the distance $d(t)$ for the $\sqrt{\text{SWAP}}$ gate is determinate.

4.5 Stern-Gerlach polarizing splitter

In an atomic interferometer, a "beam splitter" is used to split and recombine two paths. For example, an optical system uses a polarized beam splitter to control the light path depending on its polarization. The proposed system can switch, adiabatically, a single well to a double well by turning on a second optical trap next to the first one. A known example of this is the Stern-Gerlach experiment. This method is based on non-trapping atoms. We propose a new method, which is similar to Stern-Gerlach but, for a trapped single atom beam splitter.

The method starts with a single atom in the ground state and a single micro trap at $x = 0$. The state of the atom is $|\psi(t = 0)\rangle = \alpha |\downarrow\rangle_0 + \beta |\uparrow\rangle_0$. Then, a second microtrap is, adiabatically, switched on at $x = d$. At the same time, a magnetic field, with a gradient $\frac{\partial B_z(x)}{\partial x}$, is implemented. The magnetic force at each state is different based on their magnetic moment. Therefore, the state starts to oscillate with different frequencies. After a finite duration T, the states evolve to $|\psi(t = T)\rangle = \alpha |\downarrow\rangle_0 + \beta |\uparrow\rangle_1$. This scheme can be used to create a detection with spin depended. By adding to each qubit, a new microtrap to the detection translates the spin state to a spatial position.

24

4.6 $\sqrt{\text{SWAP}}$ Gate

The main goal of this work is to apply a two-qubit gate in an apparatus of ultracold atoms. To do it we need to achieve the following goals.

- Build the system and load with high fidelity a single qubit with the same initial conditions.

- Develop a single atom spin-resolved detection.

- Control the parameters of the two-qubit gate, and the interaction parameter and continuously change the distance between the qubits.

The previous two sub-sections explained the first two goals. The interaction parameter is controlled by modifying the Feshbach resonance, as shown in section 1.1.1, and the ^{40}K for our states Feshbach resonance is at 202.16G. To the induced magnetic field, the gradient coil with a Helmholtz was used with a current of approximately 110 A. The last parameter is the tunneling energy, and it is proportional to the distance between the microtraps. As explained in section 2.5, two microtraps are induced from a single beam that is divided at different angles (that translate to position) to several microtraps by AOD. Changing tthe different RF frequencies are translated a distance differently. One of the open questions is how to generate the microtrap trajectory to obtain a fast transfer to the gate and the same state at the end with high fidelity [21].

5 Summery

In conclusion, I suggest a new method of quantum computation in an ultracold fermionic system. This method requires a number of an experimental tools that can create a single atom in a microtrap, detect a single atom with spatial discrimination and spin-resolved, and control the in site interaction and the tunneling interaction. I described our new apparatus which is set up in these days. We want to measure and characterize a two new method. The first method applies a Stern Gerlach interferometer of a single atom. This method can give us a spatial distinction of the qubits. The second method creates a new platform for quantum computation and to realize a two-qubit gate with high fidelity.

References

[1] L Allen and JH Eberly Optical Resonance. Two-level atoms dover publications inc. *New York*, 1987.

[2] Rami Barends, Julian Kelly, Anthony Megrant, Andrzej Veitia, Daniel Sank, Evan Jeffrey, Ted C White, Josh Mutus, Austin G Fowler, Brooks Campbell, et al. Superconducting quantum circuits at the surface code threshold for fault tolerance. *Nature*, 508(7497):500–503, 2014.

[3] JHW Becher. *Towards Spin and Site-Resolved, Single-Atom Imaging of 6Li Atoms in a Multiwell Potential*. PhD thesis, Master thesis, Heidelberg University, 2016.

[4] Michael V Berry. Quantal phase factors accompanying adiabatic changes. *Proceedings of the Royal Society of London. A. Mathematical and Physical Sciences*, 392(1802):45–57, 1984.

[5] Lawrence W Cheuk, Matthew A Nichols, Melih Okan, Thomas Gersdorf, Vinay V Ramasesh, Waseem S Bakr, Thomas Lompe, and Martin W Zwierlein. Quantum-gas microscope for fermionic atoms. *Physical review letters*, 114(19):193001, 2015.

[6] Cheng Chin, Rudolf Grimm, Paul Julienne, and Eite Tiesinga. Feshbach resonances in ultracold gases. *Reviews of Modern Physics*, 82(2):1225, 2010.

[7] Juan I Cirac and Peter Zoller. Quantum computations with cold trapped ions. *Physical review letters*, 74(20):4091, 1995.

[8] Robert H Dicke. Coherence in spontaneous radiation processes. *Physical Review*, 93(1):99, 1954.

[9] David P DiVincenzo et al. The physical implementation of quantum computation. *arXiv preprint quant-ph/0002077*, 2000.

[10] Stephan Falke, Horst Knöckel, Jan Friebe, Matthias Riedmann, Eberhard Tiemann, and Christian Lisdat. Potassium ground-state scattering parameters and born-oppenheimer potentials from molecular spectroscopy. *Physical Review A*, 78(1):012503, 2008.

[11] Richard P Feynman. Simulating physics with computers. *International journal of theoretical physics*, 21(6):467–488, 1982.

[12] John Pagnucci Gaebler. *Photoemission spectroscopy of a strongly interacting Fermi gas*. University of Colorado at Boulder, 2010.

[13] Rudolf Grimm, Matthias Weidemüller, and Yurii B Ovchinnikov. Optical dipole traps for neutral atoms. *Advances in atomic, molecular, and optical physics*, 42:95–170, 2000.

[14] David Hayes, Paul S Julienne, and Ivan H Deutsch. Quantum logic via the exchange blockade in ultracold collisions. *Physical review letters*, 98(7):070501, 2007.

[15] Jonathan P Home, David Hanneke, John D Jost, Jason M Amini, Dietrich Leibfried, and David J Wineland. Complete methods set for scalable ion trap quantum information processing. *Science*, 325(5945):1227–1230, 2009.

[16] John Hubbard. Electron correlations in narrow energy bands. In *Proceedings of the Royal Society of London A: Mathematical, Physical and Engineering Sciences*, volume 276, pages 238–257. The Royal Society, 1963.

[17] A Imamog, David D Awschalom, Guido Burkard, David P DiVincenzo, Daniel Loss, M Sherwin, A Small, et al. Quantum information processing using quantum dot spins and cavity qed. *Physical Review Letters*, 83(20):4204, 1999.

[18] Stefan Kuhr et al. *A controlled quantum system of individual neutral atoms*. PhD thesis, Universitäts-und Landesbibliothek Bonn, 2003.

[19] Brian J Lester, Niclas Luick, Adam M Kaufman, Collin M Reynolds, and Cindy A Regal. Rapid production of uniformly filled arrays of neutral atoms. *Physical review letters*, 115(7):073003, 2015.

[20] VS Letokhov, VG Minogin, and BD Pavlik. Cooling and capture of atoms and molecules by a resonant light field. *Soviet Journal of Experimental and Theoretical Physics*, 45:698, 1977.

[21] H Ralph Lewis Jr and WB Riesenfeld. An exact quantum theory of the time-dependent harmonic oscillator and of a charged particle in a time-dependent electromagnetic field. *Journal of Mathematical Physics*, 10(8):1458–1473, 1969.

[22] Ch Monroe, DM Meekhof, BE King, SR Jefferts, WM Itano, DJ Wineland, and P Gould. Resolved-sideband raman cooling of a bound atom to the 3d zero-point energy. *Physical Review Letters*, 75(22):4011, 1995.

[23] Jeremy L O'Brien. Optical quantum computing. *Science*, 318(5856):1567–1570, 2007.

[24] Maxwell F. Parsons, Florian Huber, Anton Mazurenko, Christie S. Chiu, Widagdo Setiawan, Katherine Wooley-Brown, Sebastian Blatt, and Markus Greiner. Site-resolved imaging of fermionic ^{6}Li in an optical lattice. *Phys. Rev. Lett.*, 114:213002, May 2015.

[25] Mohit Randeria, W Zwerger, and M Zwierlein. The bcs–bec crossover and the unitary fermi gas. In *The BCS-BEC Crossover and the Unitary Fermi Gas*, pages 1–32. Springer, 2012.

[26] Carsten Robens, Stefan Brakhane, Wolfgang Alt, Felix Kleißler, Dieter Meschede, Geol Moon, Gautam Ramola, and Andrea Alberti. High numerical aperture (na= 0.92) objective lens for imaging and addressing of cold atoms. *Optics letters*, 42(6):1043–1046, 2017.

[27] Friedhelm Serwane, Gerhard Zürn, Thomas Lompe, TB Ottenstein, AN Wenz, and S Jochim. Deterministic preparation of a tunable few-fermion system. *Science*, 332(6027):336–338, 2011.

[28] Constantine Shkedrov, Yanay Florshaim, Gal Ness, Andrey Gandman, and Yoav Sagi. High sensitivity rf spectroscopy of a strongly-interacting fermi gas. *arXiv preprint arXiv:1803.01770*, 2018.

[29] JT Stewart, JP Gaebler, TE Drake, and DS Jin. Verification of universal relations in a strongly interacting fermi gas. *Physical Review Letters*, 104(23):235301, 2010.

[30] Christof Weitenberg, Stefan Kuhr, Klaus Mølmer, and Jacob F Sherson. Quantum computation architecture using optical tweezers. *Physical Review A*, 84(3):032322, 2011.

[31] David J Wineland, C Monroe, Wayne M Itano, Dietrich Leibfried, Brian E King, and Dawn M Meekhof. Experimental issues in coherent quantum-state manipulation of trapped atomic ions. *Journal of Research of the National Institute of Standards and Technology*, 103(3):259, 1998.

[32] Ryuta Yamamoto, Jun Kobayashi, Takuma Kuno, Kohei Kato, and Yoshiro Takahashi. An ytterbium quantum gas microscope with narrow-line laser cooling. *New Journal of Physics*, 18(2):023016, 2016.